De Gruyter Brill
Paradigm
ISSN 1335-8871

MEASUREMENT SCIENCE REVIEW

Journal homepage: https://reference-global.com/journal/MSR

Accuracy Improvement of DIC Method Displacement Measurement Based on Image Stabilization

Huai Yang[1,2*], Lilan Fu[1,2], Xianmao Wen[1], Lin Zhou[1] and Huan Zhang[1,2]

[1]*School of Engineering, Bijie Vocational and Technology College, Bijie, 551700, China, yanghuai01@foxmail.com*
[2]*Key Laboratory of Smart Structure Health Monitoring, Bijie, 551700, China, zhanghuan04@foxmail.com*

Abstract: Digital image correlation (DIC) is a cornerstone technique for displacement measurement, offering transformative potential for structural health monitoring (SHM) applications due to its non-contact nature and cost-effectiveness. However, in practical applications, image jitter caused by extended monitoring distances and suboptimal optical conditions degrades accuracy. Given the significant relationships among pixel resolution, stability, and DIC measurement accuracy, this paper proposes a study to improve image stability using corner detection methods to improve the measurement accuracy of DIC technology. First, a camera captures multiple dynamic displacement images of slowly moving objects at different distances. Then, image stabilization technology is applied to the images for algorithmic processing, followed by DIC analysis. The results show that under normal acquisition conditions, the relative errors of DIC-analyzed data at different distances range from 3.8 % to 8.6 %, with displacement errors increasing with distance. In contrast, the relative errors of data processed with image stabilization technology range from 3.2 % to 6.0 %, demonstrating accuracy improvements of 4.2 % to 34.1 % (the improvement in accuracy increases with increasing test distance). This indicates that image stabilization technology can effectively improve the accuracy of DIC-based displacement measurement.

Keywords: digital image correlation, corner detection, image stabilization, displacement measurement

1. INTRODUCTION

With the development of social economy, the number of newly constructed buildings continues to increase, while more aging buildings experience gradual structural deterioration. Concerns about building safety, stability, and durability have grown significantly, leading many scholars to engage in structural monitoring [1]. digital image correlation (DIC) is a non-contact measurement technology with advantages such as low cost and non-contact measurement capabilities [2]. Given that the future of structural monitoring relates to socioeconomic and public safety issues, high-precision, efficient building monitoring is essential.

Conventional approaches often rely on field instruments such as theodolites and contact-based sensors. Although these techniques are recognized for their precision, they are not without drawbacks, including significant resource allocation, extended monitoring durations, and potential disruptions to traffic flow [3]. With advancements in modern technology, new building monitoring methods, such as GPS and accelerometer-based monitoring, have emerged [4]. Although these methods exhibit high automation and efficiency, they still present notable drawbacks: the inability to perform real-time, continuous measurements; high time costs; and low accuracy in long-distance measurements [5].

This paper proposes a method to improve accuracy using image stabilization technology based on the DIC method. Compared to traditional monitoring methods, DIC technology imposes less stringent requirements on practical environments and offers advantages such as full-field measurement, high efficiency, and no effect on the normal usage of structures [6]. Digital image processing emerged in the early 1960s, and over the decades of development and extensive scholarly research, DIC technology has improved significantly [7]. DIC errors can generally be categorized into systematic errors and random errors. Systematic errors primarily arise from discrepancies between DIC processing procedures and experimental assumptions, while random errors stem from camera quality and environmental noise. These errors significantly impact the measurement accuracy and reliability of DIC systems. Wang Dongmei et al. reduced out-of-plane displacement effects by ensuring specimen planarity. Additionally, DIC requires environmental stability; Wang Dongmei's team observed that, in high-magnification tests, mechanical vibration amplitudes are amplified, prompting them to adopt methods to suppress environmental interference [8]. DIC enables rapid, continuous, fixed-point, and real-time building monitoring. However, due to practical monitoring constraints, unresolved accuracy issues persist,

DOI: 10.2478/mr-2026-0020

Corresponding author: yanghuai01@foxmail.com (Huai Yang)

particularly the impact of image jitter during displacement extraction from continuous images. To address this gap, developing a method to stabilize continuous images to improve DIC accuracy is of significant importance.

Recently, phase-based motion estimation techniques [9] have emerged as an alternative approach for high-sensitivity displacement measurement, leveraging subtle phase variations in video sequences [10] to achieve sub-pixel accuracy. These methods have demonstrated particular promise in civil infrastructure monitoring, where they enable target-free vibration measurement [11], [12] and cable force estimation [13]. However, phase-based techniques typically require high frame rates and are sensitive to motion amplitude, making them less suited for slow, large-amplitude displacements under varying lighting conditions. In contrast, the present study focuses on improving the robustness of traditional DIC by addressing a fundamental source of error — image jitter — through a corner-detection-based stabilization preprocessing step.

Corners are points in 2D images where intensity changes abruptly, or points of maximum curvature on image edge curves [14]. Since their proposal in the 1970s, corner detection has attracted increasing scholarly attention, leading to numerous extraction methods. Four representative categories include grayscale-based, binary image-based, edge feature-based, and support vector machine-based corner detection algorithms. Current mainstream methods fall into two categories: grayscale-based and edge feature-based. Edge feature-based detection identifies corners using edge characteristics, such as contour point symmetry, edge curvature, and angles. Early algorithms employed contour chain code-based methods, exemplified by the Freeman chain code analysis [15]. In 1998, Mokhtarian proposed the Curvature Scale Space (CSS) algorithm, in which corners correspond to points of maximum curvature along edges [16]. The process involves: (1) extracting edges via Canny detection, (2) calculating curvatures at multiple scales to identify candidate corners, and (3) refining corner positions by reducing scales [17]. In 2002, Mokhtarian automated threshold selection in CSS to eliminate empirical limitations. Cai et al. (2011) further improved CSS by incorporating mathematical morphology for edge extraction. Sun Bo et al. analyzed traditional algorithms, addressed their shortcomings by integrating improved Canny detection into CSS, and added pseudo-corner elimination, achieving higher precision [18]. Despite progress, applying corner detection to improve DIC accuracy remains underexplored, necessitating further research.

When using DIC methods, factors such as lighting conditions, camera technology, and equipment limitations lead to images with poor clarity and instability. These quality issues severely affect DIC algorithms' ability to extract regions of interest (ROIs), resulting in degraded dynamic displacement analysis. To improve the DIC accuracy, this study investigates whether dynamic displacement images processed with corner detection enhance precision. A strictly controlled variable approach is adopted to minimize confounding factors. The results aim to provide comprehensive insights for practical applications and to fill gaps in video-based corner detection technologies to improve DIC monitoring accuracy.

2. METHODS

To improve the accuracy of structural measurements using DIC technology, this study proposes an image stability enhancement method based on corner detection technology. The implementation of this method is divided into two modules, which include: *Module 1*: Dynamic displacement measurement of objects based on DIC technology; *Module 2*: Improvement of image jitter through corner detection and recognition using the Shi-Tomasi corner detection algorithm [19]. Actual dynamic displacement data of slow-moving objects is measured using precise instruments and compared with the proposed method for analysis.

A. DIC-based dynamic displacement measurement

In DIC-based displacement analysis, two key techniques are used for rough estimation and precise measurement: integer pixel displacement analysis [20] and sub-pixel displacement analysis [21]. Integer pixel displacement estimates optimal positions between images or frames. Although various methods exist, Fourier transform-based cross-correlation (FTCC) [22] proves more efficient. Sub-pixel displacement analysis further improves precision based on integer pixel results. The inverse compositional Gauss-Newton (IC-GN) algorithm [23] is a common sub-pixel calculation method. The technical principles are briefly described below.

Integer-pixel displacement calculation

After acquiring image sequences of the ROI, FTCC calculates integer-pixel displacements. Cross-correlation measures similarity between two signals (image sub-regions). For reference and target sub-regions with identical sizes undergoing pure x/y displacement, the displacement expression is:

$$f_2(x, y) = f_1(x - u, y - v) \tag{1}$$

Using 2D Fourier transforms into reference (F) and target (G) sub-regions:

$$F_2(\varepsilon, \eta) = e^{-j2\pi(\varepsilon u + \eta v)} F_1(\varepsilon, \eta) \tag{2}$$

where F_1 and F_2 are Fourier transforms of f_1 and f_2; ε and η are frequency coordinates; j is the imaginary unit.

Given that the Fourier transform spectrum undergoes modification solely in the phase, it can be deduced that only a phase difference pertaining to the displacement (u, v) exists. In accordance with the frequency domain properties, the mutual correlation of two functions can be realized in the frequency domain through the conjugate multiplication of the Fourier transform of one function with the Fourier transform of the other function:

$$F_{corr}(\varepsilon, \eta) = F_1(\varepsilon, \eta) \cdot F_2^*(\varepsilon, \eta) \tag{3}$$

where $F_{corr}(\varepsilon, \eta) = e^{-j2\pi(\varepsilon u + \eta v)}$; $F_2^*(\varepsilon, \eta)$ is the complex conjugate of $F_2(\varepsilon, \eta)$.

The inverse Fourier transform of the result in the above equation yields the impulse function, a two-dimensional array of peak locations corresponding to whole-pixel displacements between the two sub-regions. By identifying the peaks at their respective locations, the magnitude of the whole-pixel displacement of the target sub-region relative to the reference sub-region can be determined.

Sub-pixel displacement calculation

Sub-pixel displacement calculation further refines accuracy below one pixel using the IC-GN algorithm, which minimizes grayscale residuals.

The grayscale residual is defined as $e(x,y;p) = J(T(x,y;p)) - I(x,y)$, and the objective is to find a set of parameters p such that the residual $e(x,y;p)$ minimizes the sum of squares over the entire sub-region, i.e., $min_p \sum_{x,y} e^2\,(x,y;p)$. The IC-GN algorithm is an iterative optimization algorithm for solving the above minimization problem. In each iteration, the nonlinear minimization problem is transformed into a linear least squares problem by linearizing the approximation of the residual $e(x,y;p)$ function with respect to the parameter p.

Using FTCC-derived integer displacement as the initial value, zero-mean normalized sum of squared differences (ZNSSD) [24] serves as a correlation criterion:

$$C_{ZNSSD} = \sum \left\{ \frac{[f(x,y)] - f_m}{\sqrt{\sum [f(x,y) - f_m]^2}} - \frac{[g(x',y')] - g_m}{\sqrt{\sum [g(x',y') - g_m]^2}} \right\}^2 \tag{4}$$

where: $f(x,y)$ and $g(x',y')$ are the 2D grayscale functions of the reference sub-region and the target sub-region, respectively; (x,y) and (x',y') are the coordinates of the 2D grayscale functions; f_m and g_m are the mean values of $f(x,y)$ and $g(x',y')$, respectively. When the IC-GN algorithm iteratively converges to the minimum value in the previous equation, the sub-pixel displacement results in the image can be obtained.

The combination of FTCC and IC-GN enables high-precision displacement measurement in DIC.

B. Corner detection and recognition using the Shi-Tomasi algorithm

Unprocessed images in structural measurements introduce jitter-induced errors during analysis. Building on the Harris algorithm, the Shi-Tomasi method imposes a minimum inter-feature distance constraint, thereby ensuring a more uniform distribution of detected corners. Its principles are:

Step 1:

Convert the input image to grayscale.

Step 2:

Compute x/y gradients using the Sobel operator, obtaining the gradient magnitude (A) and direction (B). Calculate the autocorrelation matrix M for each pixel:

$$\begin{aligned} E(u,v) &= \sum_{x,y} \omega(x,y)\,[\,I(x+u,\ \ y+u) - I(x,y)]^2 \\ &= \sum_{x,y} \omega(x,y)\,[(x,y) + I_x u + I_y u - I(x,y)]^2 \\ &= \sum_{x,y} \omega(x,y)[I_x^2\,u^2 + 2I_x I_y uv + I_y^2 v^2] \\ &= \sum_{x,y} \omega(x,y)[u,v] \begin{bmatrix} I_x^2, & I_x I_y \\ I_x I_y, & I_y^2 \end{bmatrix} \begin{bmatrix} u \\ v \end{bmatrix} \\ &= [u,v] \sum_{x,y} \omega(x,y) \begin{bmatrix} I_x^2, & I_x I_y \\ I_x I_y, & I_y^2 \end{bmatrix} \begin{bmatrix} u \\ v \end{bmatrix} \\ &= [u,v]\, M \begin{bmatrix} u \\ v \end{bmatrix} \end{aligned} \tag{5}$$

$$M = \sum (\,\omega(x,y)\ \cdot\ [I_x^2, I_x \cdot I_y;\ I_x \cdot I_y, I_y^2]) \tag{6}$$

where M is considered as a function of I_x and I_y, it possesses two distinct eigenvalues, λ_1 and λ_2. In the scenario where λ_1 and λ_2 assume large and approximately equal values, it is regarded as a corner point in the image. The $\omega(x,y)$ window function plays a pivotal role in the selection of a region of interest (ROI) within the structure depicted in the image. This function calculates the weighting of the localized region, thereby contributing to the overall analysis. Notable window functions include the rectangular window and the Gaussian window.

Step 3:

Compute eigenvalues λ_1, λ_2 of M. The Shi-Tomasi response function uses $R = min\,(\lambda_1, \lambda_2)$, outperforming Harris' [25] $R = \lambda_1\lambda_2 - K(\lambda_1 + \lambda_2)^2$ in stability and accuracy.

In our experiments, the Shi-Tomasi corner detector was configured with the following parameters: maximum number of corners $N = 100$, quality level threshold $= 0.5$, minimum Euclidean distance between corners $= 2$ pixels. The window function used was a Gaussian window of size 5×5. These values were chosen to ensure a sufficient number of stable corners while avoiding clustering, based on preliminary tests. A simplified image stabilization workflow consists of the following steps:

Step 4:

Sort corner responses and select the top N corners.

The efficacy of the Shi-Tomasi method in addressing corner point jitter issues is evident when compared with the original image. In addition, this study uses the ROI rectangular box to ensure the stability of corner point selection in the local area of the image (to avoid moving objects). The objective is to fix the image of the region. The corner point of the region is applied to the entire image across different frames, thereby achieving a substantial effect on the image. The objective is to stabilize the region within the image and then use the corner points of the region across different frames of the entire image to address the jitter issue.

3. RESULTS

To verify the feasibility of the proposed method, on-site collection of displacement image data was conducted. The designed experimental test distance combinations: 30 m, 45 m, 60 m, 75 m, 90 m. First, the identified object was slowly moved from right to left within the field of camera view, requiring relatively stable reference markers in the frame to capture stable corner points using corner detection techniques. An 80 mm × 80 mm target marker was attached to the object surface for recognition framing. The object was positioned directly in front of the camera and moved regularly and slowly at different distances. The test sets are shown in Fig. 1. The camera captured image sequences during movement. To minimize the impact of lighting variations on system measurement accuracy, the camera was recalibrated every 60 seconds. According to the Shannon Sampling Theorem, the system sampling frequency was set to 30 Hz to avoid signal distortion during analog signal recovery. The integrated acquisition system featured a resolution of 3072 × 2048 pixels and a focal length of 120 mm. To ensure data validity, a traditional experimental design methodology was used, strictly implementing experimental and control groups.

Fig. 1. Test sets.

To validate the proposed algorithm and ensure the accuracy of DIC data, image data of moving objects was collected at different distances. Experiments were conducted at distances of 30.137 m, 45.046 m, 60.097 m, 75.062 m, and 90.256 m, with the objects positioned directly facing the camera and moving slowly in a horizontal direction. The displacement magnitudes of the object were sequentially reduced as follows: 300 mm, 200 mm, 100 mm, 50 mm, 30 mm, 10 mm, 5 mm, and 3 mm. To ensure true displacement measurements, a rangefinder was used to record each displacement during the experiments. Dynamic displacement tests were performed on objects at different distances, resulting in five groups, to ensure the accuracy and reliability of the experimental data.

A. Displacement data acquisition based on the DIC method

After obtaining displacement data of the moving object using corner detection techniques, preprocessing is required, including the extraction and organization of valid data. For data processing, the first trial (where the object was moved 300 mm at a distance of 30 m) is illustrated in Fig. 2.

It can be observed that in unprocessed DIC images, the displacement results from the DIC method exhibit noticeable jitter, whereas DIC results processed with image stabilization show better consistency. This indicates that image stabilization provides an effective means to stabilize pixel displacements in dynamic image analysis.

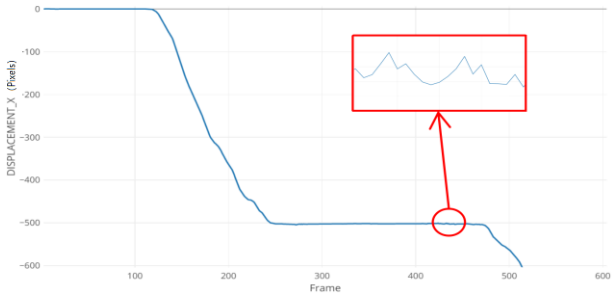

(a) Before image stabilization

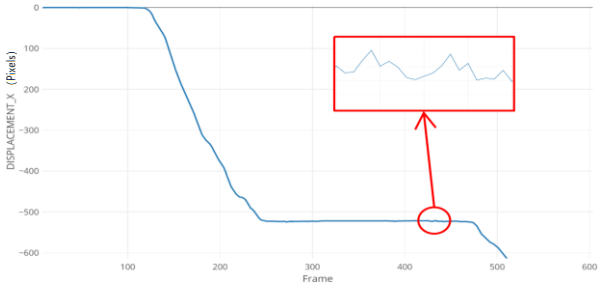

(b) After image stabilization

Fig. 2. Comparison of the displacement curve between before and after image stabilization at 30 m.

To investigate the influence of image stabilization DIC displacement measurement accuracy, the relative errors were analyzed using multiple sets of dynamic displacement data at different distances. The distances were divided into 5 groups (different distances): 30.173 m (2 groups), 45.046 m (2 groups), and 60.097 m (2 groups), along with the actual displacement. The relevant parameters for calculating relative errors are presented in Table 1, where:

L represents the actual displacement distance of the target;

L_1 indicates the pixel displacement measured by the DIC method;

L_2 indicates the pixel displacement after corner detection processing.

Table 1. Calculation parameters of tests at 30 m.

Counts	L [mm]	L_1 [mm]	L_2 [mm]
1	295	283.60	294.99
2	205	190.85	198.48
3	102	91.82	94.53
4	49	48.21	51.08
5	34	30.67	31.90
6	10	10.00	10.40
7	5	5.20	5.42
8	3	2.96	3.08

Comparison of actual displacement, DIC-measured displacement, and DIC-measured displacement after image stabilization results for 5 groups are plotted in Fig. 3.

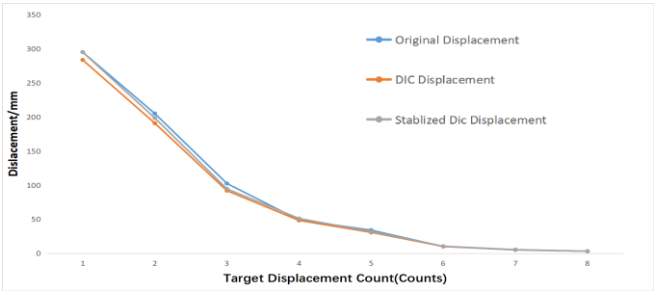

(a) Distance: 30.173 m

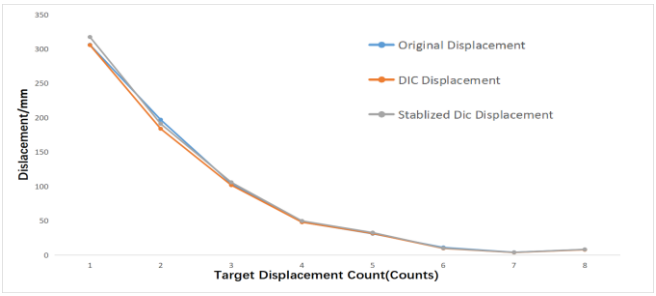

(b) Distance: 45.046 m

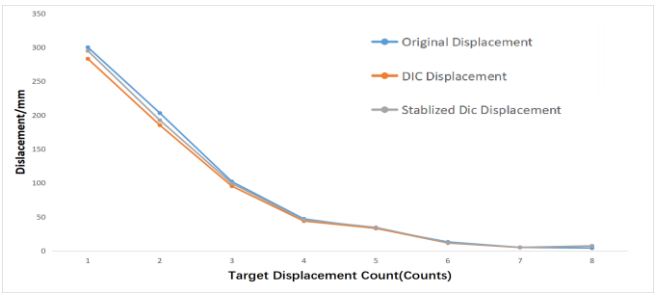

(c) Distance: 60.097 m

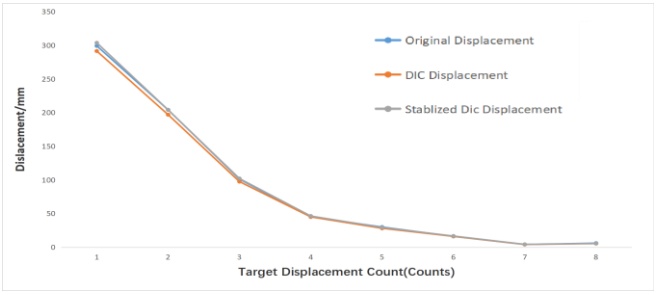

(d) Distance: 75.062 m

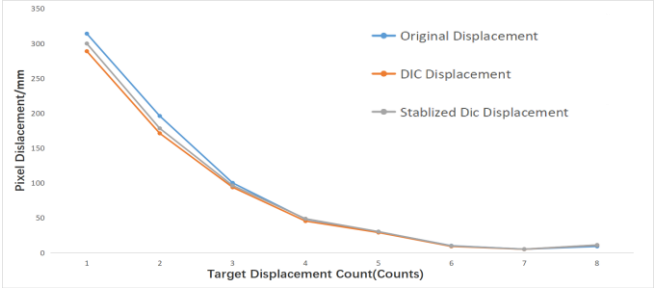

(e) Distance: 90.256 m

Fig. 3. Displacement curves of each segment under varying distances.

As shown in Fig. 3, the displacement curves at different distances — after image stabilization processing — show DIC displacement results that are closer to the actual displacement curves compared to the original DIC displacement results.

B. Accuracy analysis of dynamic displacement curves

Through systematic calculations, the relative errors in the displacements obtained by the DIC method ranged from 4.1 % to 8.6 %. After stabilization processing, the relative errors in the displacements were reduced to 4.5 %-6.0 %. Overall, accuracy showed significant improvement after stabilization processing. As shown in Table 2, ω_1 and ω_2 are the mean relative errors pre- and post-stabilization, and φ quantifies their reduction rate.

Table 2. Average relative errors at different distances.

Distance [m]	ω_1 [%]	ω_2 [%]	φ [%]
30.173	4.7	4.5	4.2
45.046	4.1	3.8	7.3
60.097	7.5	6.0	20.0
75.062	3.8	3.2	14.9
90.256	8.6	5.6	34.1

As shown in Fig. 4, an exponential regression of the mean relative error against distance was performed to characterize the distance-dependent trend. For the raw DIC data, the fitted model is $y = 0.1244e^{0.029x}$ ($R^2 = 0.5605$), while for the stabilized data, the model is $y = 0.0793e^{0.0279x}$ ($R^2 = 0.559$). Here x represents the test distance in meters, and y denotes the mean relative error. The lower growth coefficient after stabilization suggests that the proposed method partially mitigates the increase in distance-induced error. Although the limited number of measurement distances (five) and the inherent variability in field tests result in moderate R^2 values, these preliminary models offer a useful reference for estimating measurement uncertainty across different ranges. Further experiments with more distance intervals would help establish more robust predictive models.

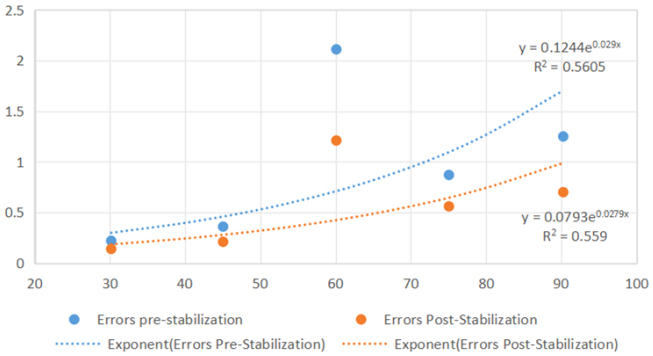

Fig. 4. Exponential regression of mean relative error against test distance for raw DIC and stabilized DIC measurements.

In addition to mean relative errors, the standard deviation (SD) of displacement errors was calculated for each distance to assess measurement consistency, as shown in Table 3.

σ_1 and σ_2 are the SD values of pre- and post-stabilization, and λ quantifies their reduction rate. The figures confirmed that image stabilization not only reduces the mean error but also improves repeatability, with error variability decreasing by an average of 36.4-45.5 % across all distances.

Table 3. Standard deviation of measurement errors at different distances.

Distance [m]	σ_1 [pixels]	σ_2 [pixels]	Λ [%]
30.173	0.22	0.14	36.4
45.046	0.36	0.21	41.6
60.097	2.11	1.21	43.1
75.062	0.87	0.56	35.6
90.256	1.25	0.70	45.5

The following findings can be observed: Under the same distance conditions, the processed result's average error rate is significantly lower than that of the unprocessed result. Generally, as distance increases, the displacement average error gradually increases. This occurs because the original image exhibits greater jitter at longer distances due to various interference factors. Image stabilization processing demonstrates superior error reduction performance at longer distances than at shorter distances.

4. Conclusion

In this investigation, we introduce a novel approach that leverages corner detection algorithms to enhance the precision of DIC for displacement measurement. Based on the analysis and discussion of experimental results, the following conclusions are drawn:

A. Improved DIC accuracy with image stabilization

The application of corner detection technology significantly improves measurement accuracy compared to unprocessed image data. This improvement is attributed to the use of edge feature points in corner detection, which calculates and adjusts positional changes across video frames. By mitigating inter-frame jitters in stabilized video inputs, the processed data reduces the adverse effects of raw video instability on DIC, thereby improving its precision.

B. Distance-dependent effectiveness

Improvement rates at increasing distances (from near to far) range from 4.2 % to 34.1 %. This trend demonstrates that image stabilization technology achieves superior performance in long-distance structural monitoring using DIC, with effectiveness escalating proportionally to distance.

C. Limitations and future directions

While corner detection effectively addresses minor video jitter, experiments revealed that processing distant images containing atmospheric turbulence-induced optical distortions unexpectedly exacerbates jitter. Future research should prioritize methods to reduce such optical distortions caused by atmospheric factors, thereby minimizing their impact on image stability and DIC accuracy.

Funding

This work is supported by: (1) Research Teams Program and College Research Programs of Bijie Vocational and Technical College, (2) Bijie City Joint Fund Project: Research on the Accuracy of Long-Distance Structural Displacement Monitoring Based on Machine Vision, (3) Bijie Vocational and Technical College Fund Project- Research on Key Issues of Displacement Monitoring Accuracy Based on DIC.

Data availability statement

The data presented in this study are available from the corresponding author upon reasonable request.

Acknowledgment

The authors declare no conflicts of interest. The funders had no role in the design of the study, the collection, analysis, and interpretation of data, the writing of the manuscript, or the decision to publish the results.

References

[1] Biondini, F., Frangopol, D. M. (eds.) (2012). *Bridge Maintenance, Safety, Management, Resilience and Sustainability*. CRC Press. https://doi.org/10.1201/b12352

[2] Farrar, C. R., Worden, K. (2007). An introduction to structural health monitoring. *Philosophical Transactions of the Royal Society A*, 365 (1851), 303-315. http://doi.org/10.1098/rsta.2006.1928

[3] Zhou, X. (2024). Application and benefit evaluation of unmanned aerial vehicles (UAVs) in railway construction surveying. *Engineering Technology Research*, 6 (3), 1-2.

[4] Niu, Y., Li, J., Zhou, S., Liu, G., Xiang, Y., Zhang, H., Shu, J. (2023). Dynamic displacement estimation and modal analysis of long-span bridges integrating multi-GNSS and acceleration measurements. *Journal of Infrastructure Preservation and Resilience*, 4 (9). https://doi.org/10.1186/s43065-023-00077-6

[5] Li, L. (2023). Application of GPS technology in engineering survey. *Geological and Mineral Surveying and Mapping*, 6 (4), 81-83. https://doi.org/10.12238/gmsm.v6i4.1547

[6] Fang, X.-Y., Gong, J.-E., Huang, W., Wu, J.-H., Ding, J.-J. (2023). Novel characterizations of effective SIFs and fatigue crack propagation rate of welded rail steel using DIC. *Metals*, 13 (2), 227. https://doi.org/10.3390/met13020227

[7] Xu, Y., Cai, Y., Li, D., Zhang, T. (2020). Building crack monitoring based on digital image processing. *Fracture and Structural Integrity*, 14 (52), 1-8. https://doi.org/10.3221/IGF-ESIS.52.01

[8] Meng, W., Bachilo, S. M., Weisman, R. B., Nagarajaia, S. (2024). A review: Non-contact and full-field strain mapping methods for experimental mechanics and structural health monitoring. *Sensors*, 24 (20), 6573. https://doi.org/10.3390/s24206573

[9] Luo, K., Kong, X., Wang, X., Jiang, T., Frøseth, G. T., Rønnquist, A. (2023). Cable vibration measurement based on broad band phase based motion magnification and line tracking algorithm. *Mechanical Systems and Signal Processing*, 200, 110575. https://doi.org/10.1016/j.ymssp.2023.110575

[10] Luo, K., Kong, X., Zhang, J., Hu, J., Li, J., Tang, H. (2023). Computer vision-based bridge inspection and monitoring: A review. *Sensors*, 23 (18), 7863. https://doi.org/10.3390/s23187863

[11] Luo, K., Kong, X., Deng, L., Ji, W., Meng, L. (2024). Target free measurement of cable forces based on computer vision and equivalent frequency difference. *Engineering Structures*, 314, 118390. https://doi.org/10.1016/j.engstruct.2024.118390

[12] Luo, K., Kong, X., Ke, S., Hu, J., Deng, L. (2026). Target-free measurement of cable forces based on video motion magnification and high-order mode shapes. *Mechanical Systems and Signal Processing*, 247, 113966. https://doi.org/10.1016/j.ymssp.2026.113966

[13] Luo, K., Kong, X., Li, J., Hu, J., Deng, L. (2024). Motion magnification for video based vibration measurement of civil structures: A review. *Mechanical Systems and Signal Processing*, 220, 111681. https://doi.org/10.1016/j.ymssp.2024.111681

[14] Dong, L.-H., Peng, Y.-X., Fu, L.-M. (2019). Circular Harris corner detection algorithm based on Sobel edge detection. *Journal of Xi'an University of Science and Technology*, 39 (2). https://doi.org/10.13800/j.cnki.xakjdxxb.2019.0227

[15] Liu, X. H., Wang, T., Zhang, X. Z. (2018). Corner detection algorithm based on freeman code analysis. *Computer Systems and Applications*, 27 (4), 202-208. https://doi.org/10.15888/j.cnki.csa.006314

[16] Mokhtarian, F., Suomela, R. (1998). Robust image corner detection through curvature scale space. *IEEE Transactions on Pattern Analysis and Machine Intelligence*, 20 (12), 1376-1381. https://doi.org/10.1109/34.735812

[17] Wang, L., Sun, Y. (2021). Improved Canny edge detection algorithm. In *2021 2nd International Conference on Computer Science and Management Technology (ICCSMT)*. IEEE, 414-417. https://doi.org/10.1109/ICCSMT54525.2021.00081

[18] Zeng, Z., Jiang, Z., Chen, Q., He, P. (2012). An improved corner detection algorithm based on Harris. *Advanced Engineering Forum*, 6-7, 717-721. https://doi.org/10.4028/www.scientific.net/AEF.6-7.717

[19] Shi, J., Tomasi. (1994). Good features to track. In *1994 Proceedings of IEEE Conference on Computer Vision and Pattern Recognition*. IEEE, 593-600. https://doi.org/10.1109/CVPR.1994.323794

[20] Chen, Q., Tie, Z., Hong, L., Qu, Y., Wang, D. (2022). Improved search algorithm of digital speckle pattern based on PSO and IC- GN. *Photonics*, 9 (3), 167. https://doi.org/10.3390/photonics9030167

[21] Pan, B., Xie, H., Dai, F. (2007). An investigation of sub-pixel displacements registration algorithms in digital image correlation. *Chinese Journal of Theoretical and Applied Mechanics*, 23 (2), 245-252. https://doi.org/10.3321/j.issn:0459-1879.2007.02.014

[22] Fung, W.-Y., Woo, Y.-P., Liong, M.-T. (2008). Optimization of growth of *Lactobacillus acidophilus* FTCC 0291 and evaluation of growth characteristics in soy whey medium: A response surface methodology approach. *Journal of Agricultural and Food Chemistry*, 56 (17), 7910-7918. https://doi.org/10.1021/jf801567j

[23] Tian, L., Pan, B. (2016). Remote bridge deflection measurement using an advanced video deflectometer and actively illuminated LED targets. *Sensors*, 16 (9), 1344. https://doi.org/10.3390/s16091344

[24] Zhao, J., Sang, Y., Duan, F. (2019). The state of the art of two-dimensional digital image correlation computational method. *Engineering Reports*, 1 (2), e12038. https://doi.org/10.1002/eng2.12038

[25] Chen, Z., Guo, F., Luo, L. (2024). Vehicle speed measurement technologies in Intelligent Transportation Systems: Current status, challenges and future directions future directions. *Artificial Intelligence and Autonomous Systems*, 1 (2), 0004. https://doi.org/10.55092/aias20240004

Received June 11, 2025
Accepted April 14, 2026